ADVANCED MATERIALS

Supporting Information

for *Adv. Mater.,* DOI: 10.1002/adma.202104623

High-Conductive Protonated Layered Oxides from H_2O Vapor-Annealed Brownmillerites

Songbai Hu, Yuanmin Zhu, Wenqiao Han, Xiaowen Li, Yanjiang Ji, Mao Ye, Cai Jin, Qi Liu, Sixia Hu, Jiaou Wang, Junling Wang, Jiaqing He, Claudio Cazorla, and Lang Chen**

Supporting Information for

High-conductive protonated layered-oxides from H_2O vapor-annealed brownmillerites

Songbai Hu, Yuanmin Zhu, Wenqiao Han, Xiaowen Li, Yanjiang Ji, Mao Ye, Cai Jin, Qi Liu, Sixia Hu, Jiaou Wang, Junling Wang, Jiaqing He, Claudio Cazorla, Lang Chen

Correspondence to: claudio.cazorla@upc.edu and chenlang@sustech.edu.cn

This Supporting Information includes:

Figure S1 to S21

Table S1

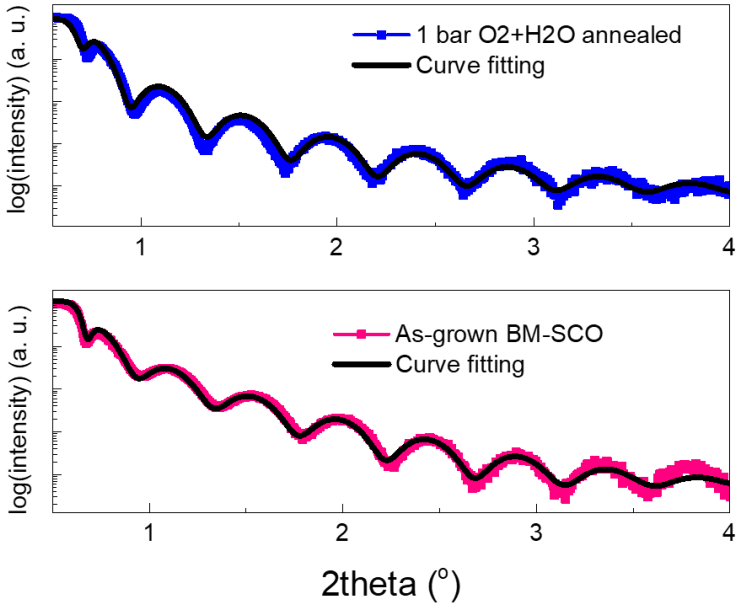

Figure S1. XRR of as-grown and 1 bar O_2 + H_2O annealed BM-SCO thin films grown on (001) LSAT substrates. Their thicknesses are determined to be 19.27 nm and 18.66 nm, respectively.

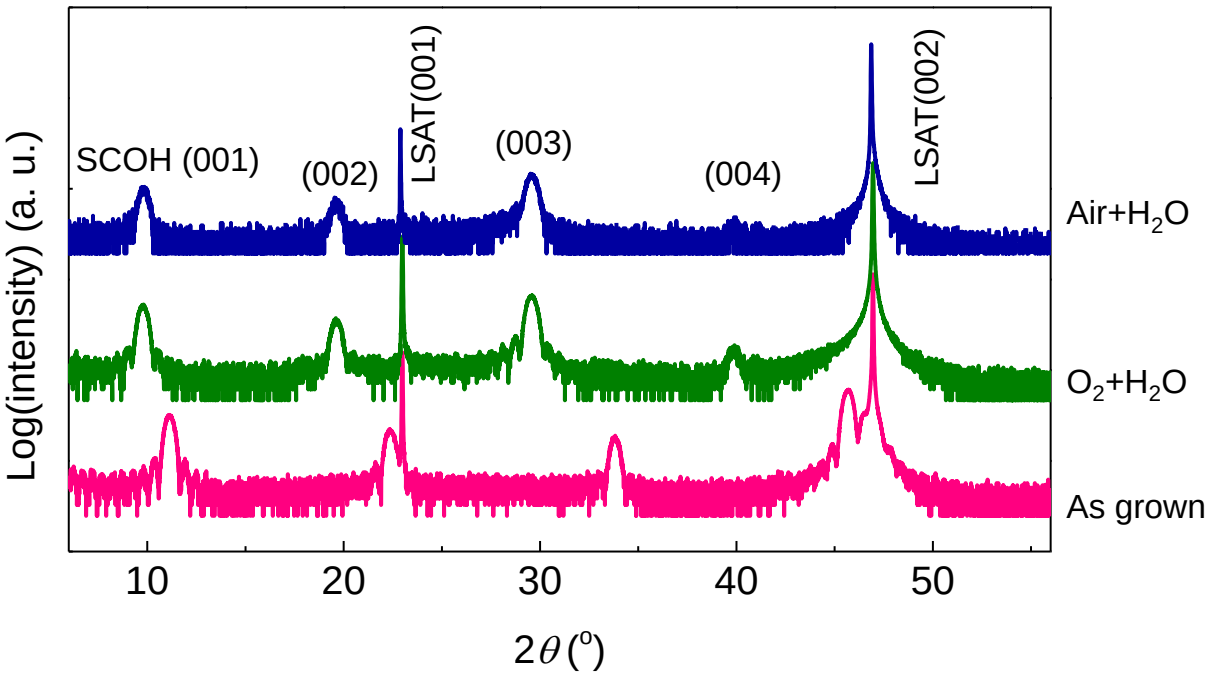

Figure S2. XRD θ-2θ scans for 1 bar O_2+H_2O and 1 bar air+H_2O annealed BM-SCO thin films.

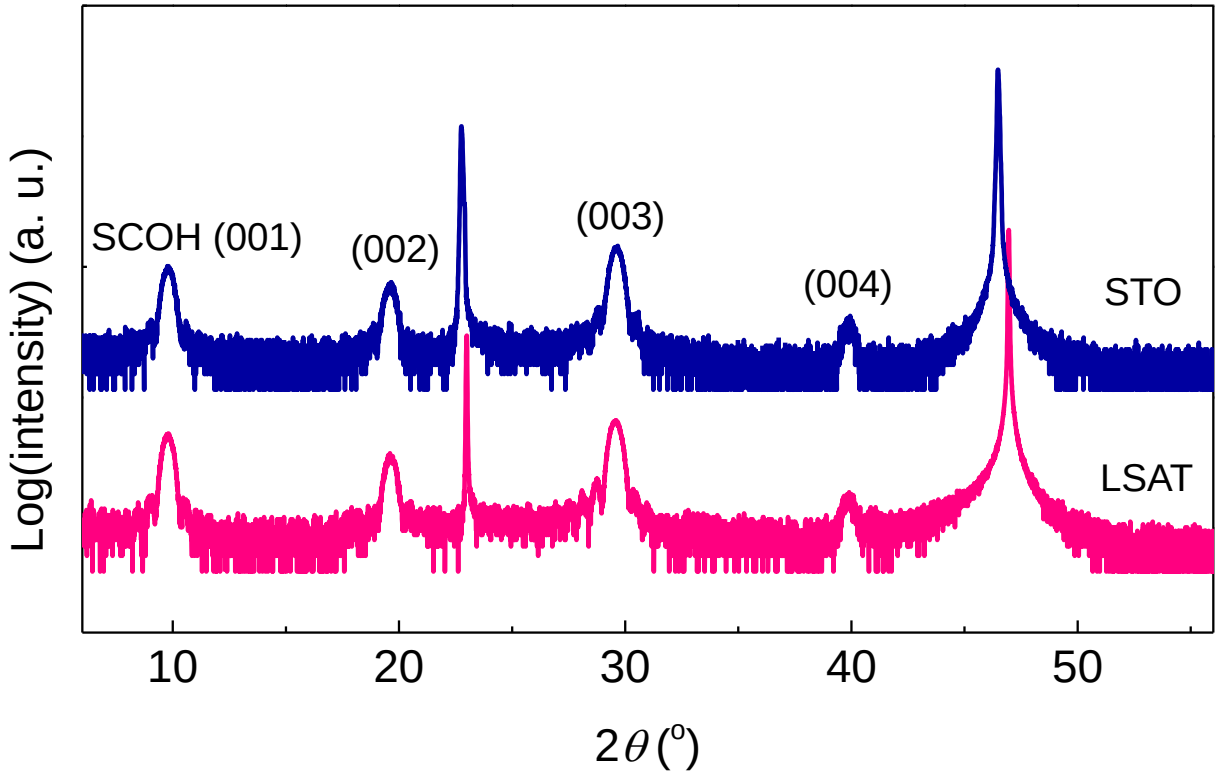

Figure S3. XRD θ-2θ scans for 1 bar O_2+H_2O annealed BM-SCO thin films grown on LSAT and STO substrates.

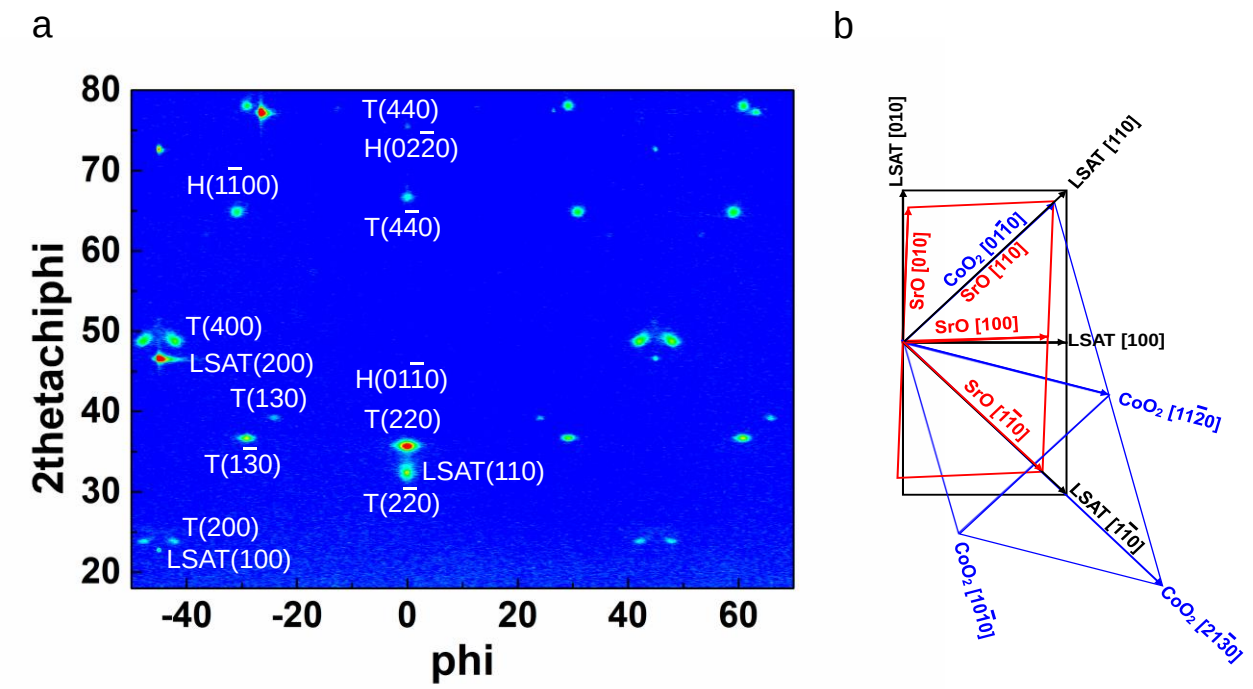

Figure S4. a) XRD in-plane $2\theta\chi\phi$ mapping of SCOH thin film grown on LSAT substrate. The 2θ angles for T (400), H (10$\bar{1}$0) and H (01$\bar{1}$0) are 48.8^o, 35.67^o and 36.82^o, respectively. The in-plane lattice constants were calculated using the γ angles measured in Figures. S5 & S6. b) The crystallographic geometry and epitaxial relationship between the SrO, CoO_2 and LSAT substrate.

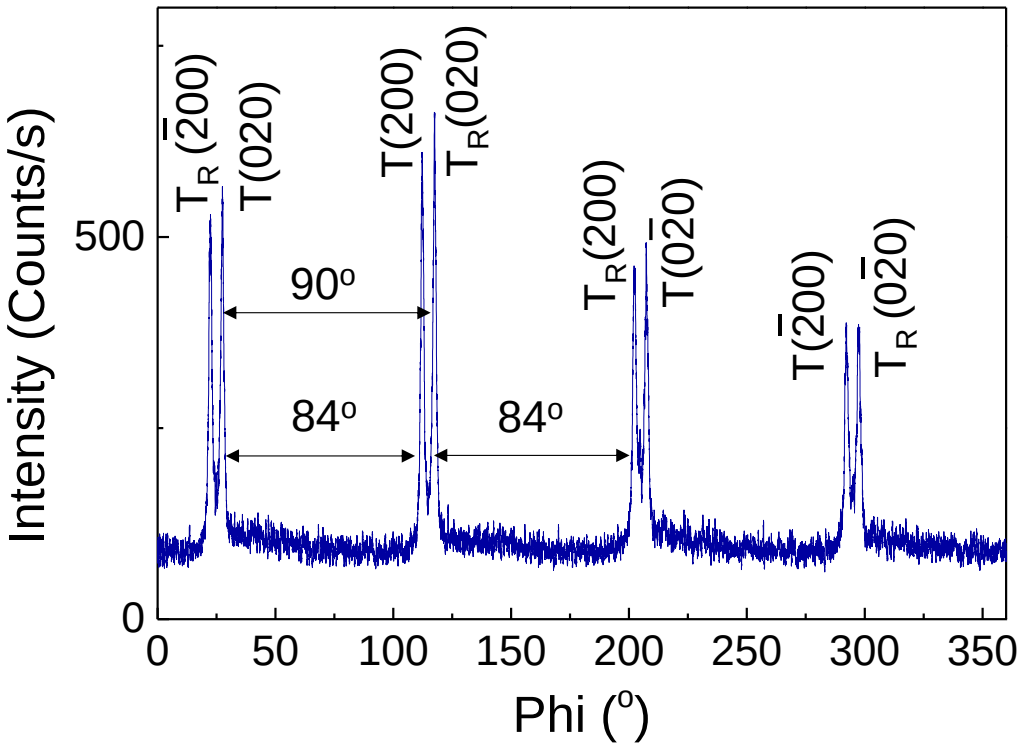

Figure S5. XRD in-plane phi-scan of SCOH thin film along the T (200) direction. The angle between T (200) and T (020) is 84°. The angle between T phase and its rotation counterpart (T_R) is 90°.

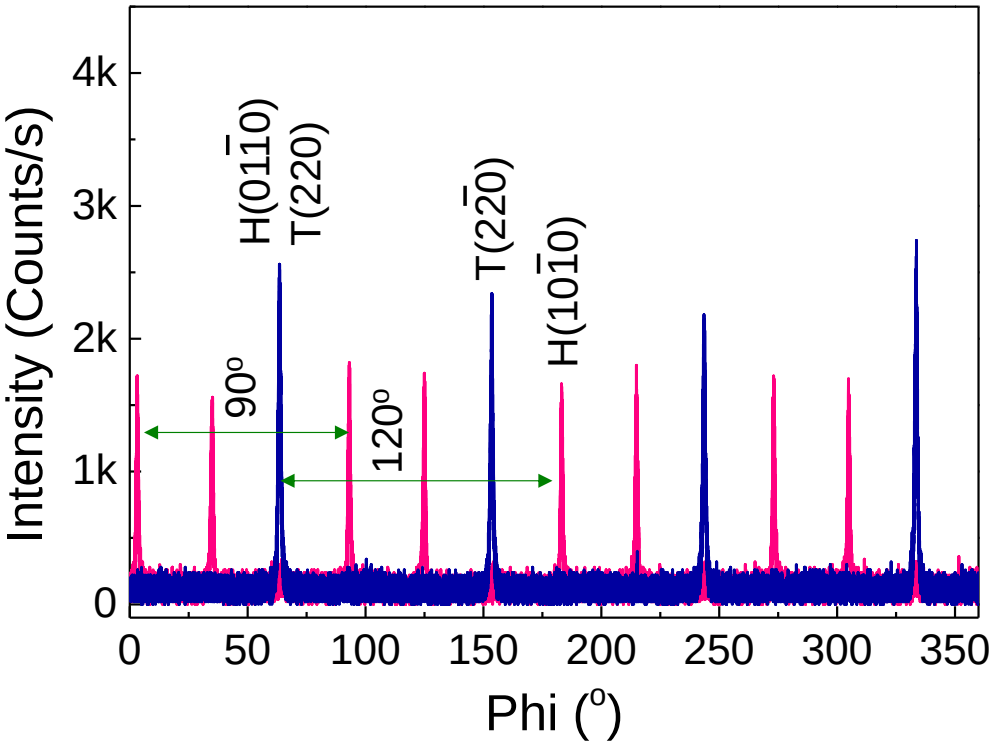

Figure S6. XRD in-plane phi-scan of SCOH thin film along the T (220) (royal blue) and H (01$\bar{1}$0) (pink) direction. The overlapping of T (220) and H (01$\bar{1}$0) azimuth indicates they have the same epitaxial direction which parallels to the LSAT [110] direction. The angle between the pseudo-hexagonal H (01$\bar{1}$0) and H (10$\bar{1}$0) is 120°. Following the T-SCO, H-SCO rotates 90° as well.

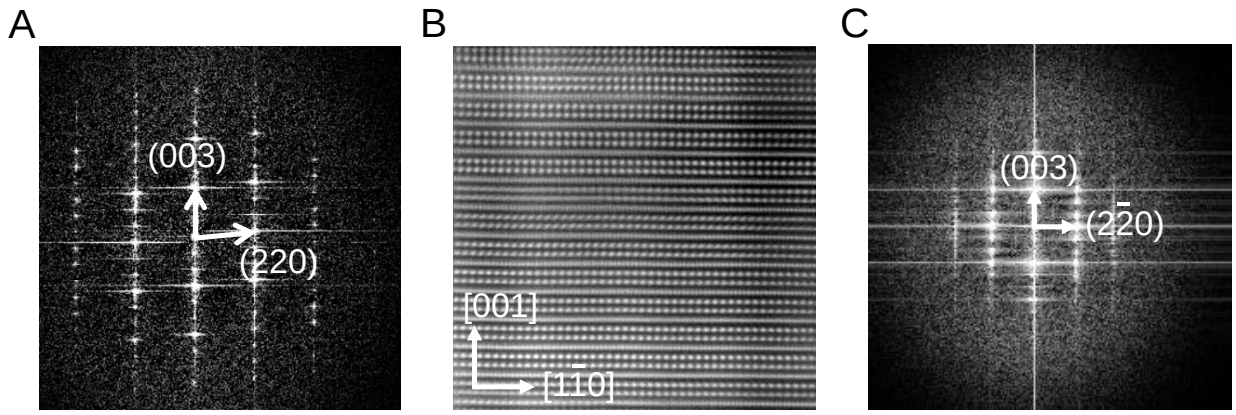

Figure S7. (A) FFT of the SCOH (220) plane in Figure 1D. (B) HADDF-STEM image and corresponding FFT of SCOH (2$\bar{2}$0) plane (C). The angles β and α of the orthogonalized SCOH are determined to be 95.5^{o} and 90°, respectively.

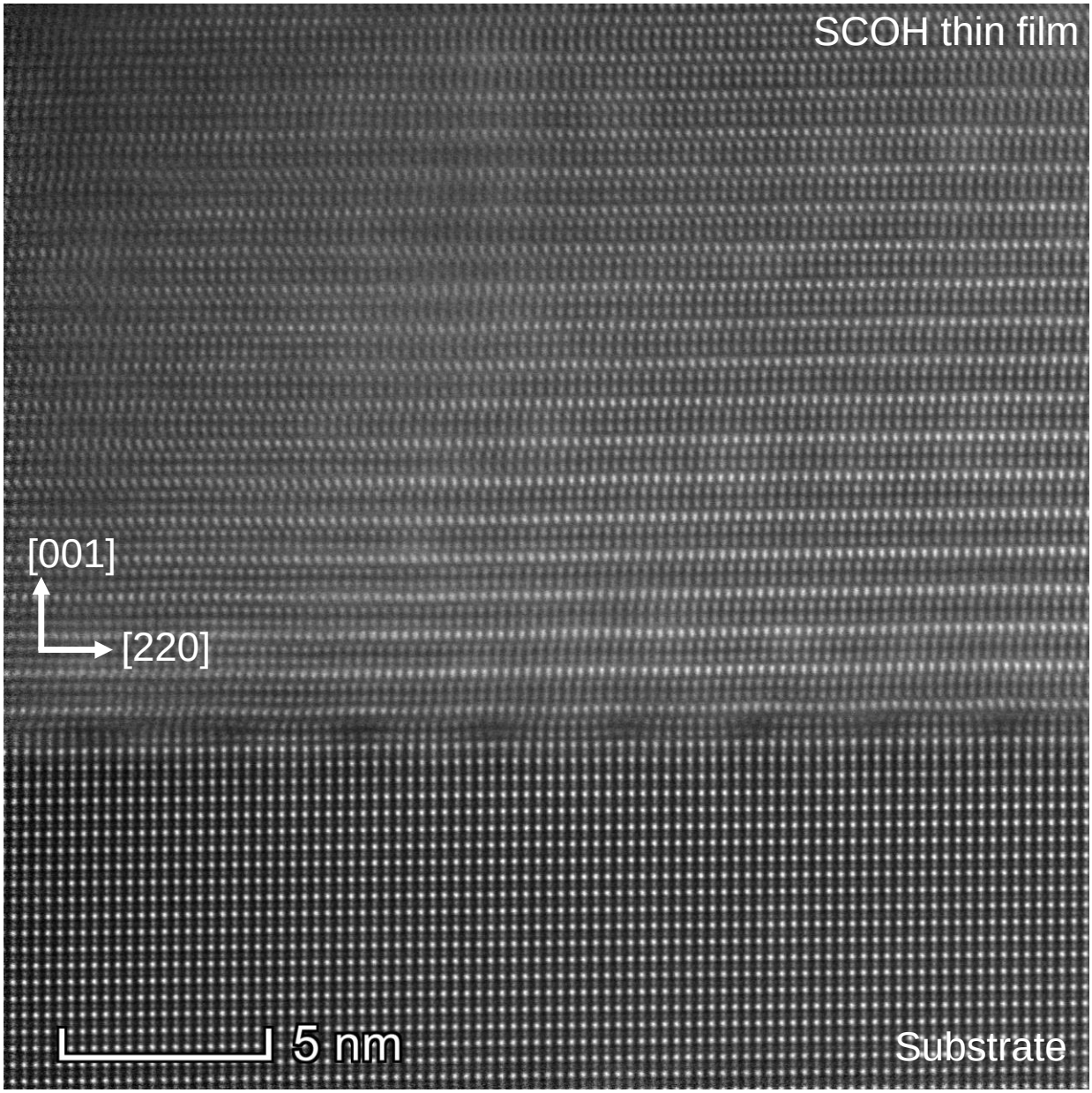

Figure S8. HADDF-STEM image of the SCOH/substrate interface. The periodical stacking faults at the interface relaxed the strain between the SCOH thin film and the substrate.

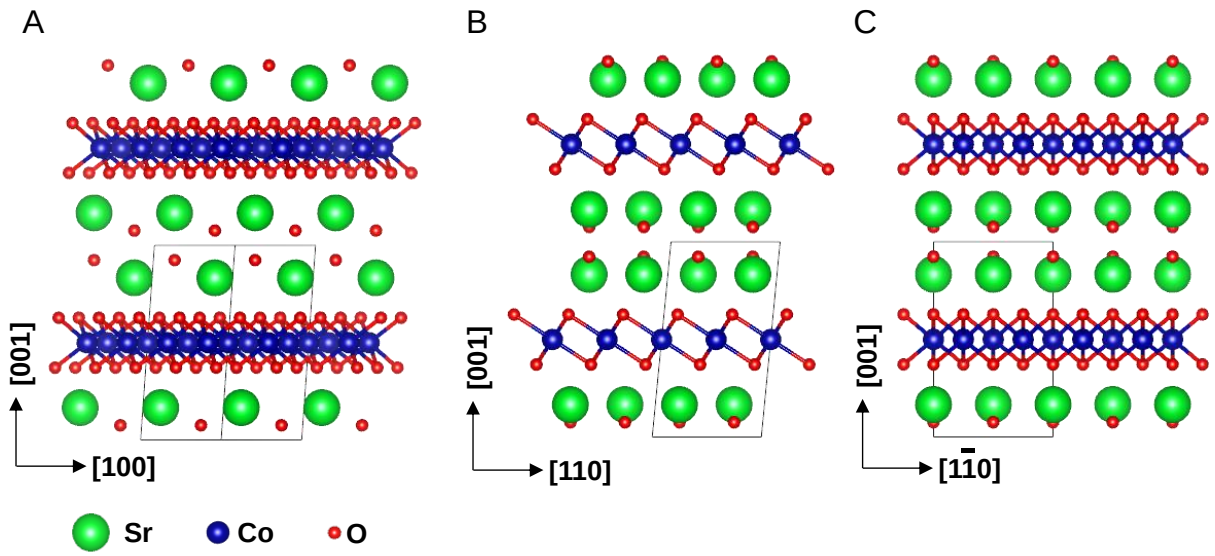

Figure S9. The atomic structure of $SrCoO_3$. The T (200), T (220) and T (2$\bar{2}$0) planes are shown in (A), (B) and (C), respectively.

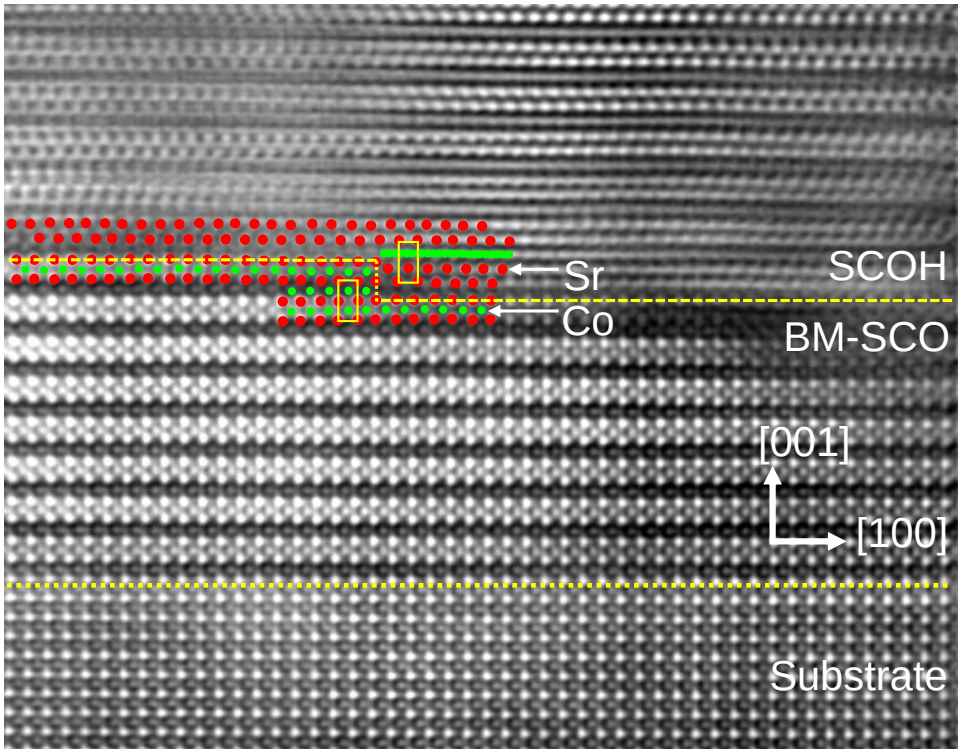

Figure S10. The reaction interface of the BM-SCO to SCOH phase transformation. The SCOH looks blurry because the SCOH (100) is 3° off the BM-SCO (100). The interface is atomically sharp and parallel to the film/substrate interface, indicating a two-dimensional layer-by-layer reaction mode.

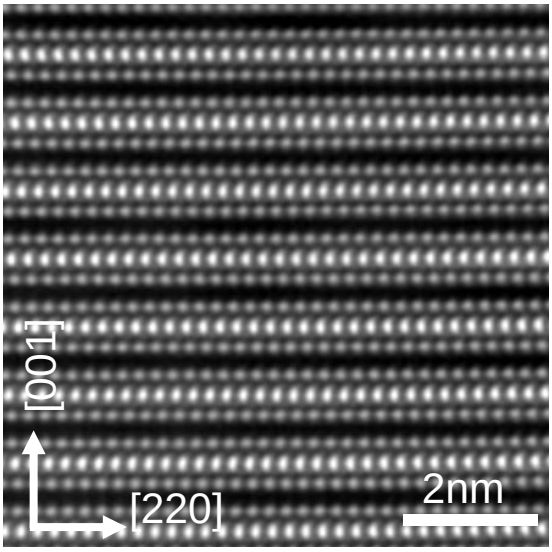

Figure S11. HADDF-STEM images of dehydrated SCOH (220) plane. A broadened gap was observed within the Sr_2O_2 layers, corresponding to the *c*-lattice constant skip at 550 °C.

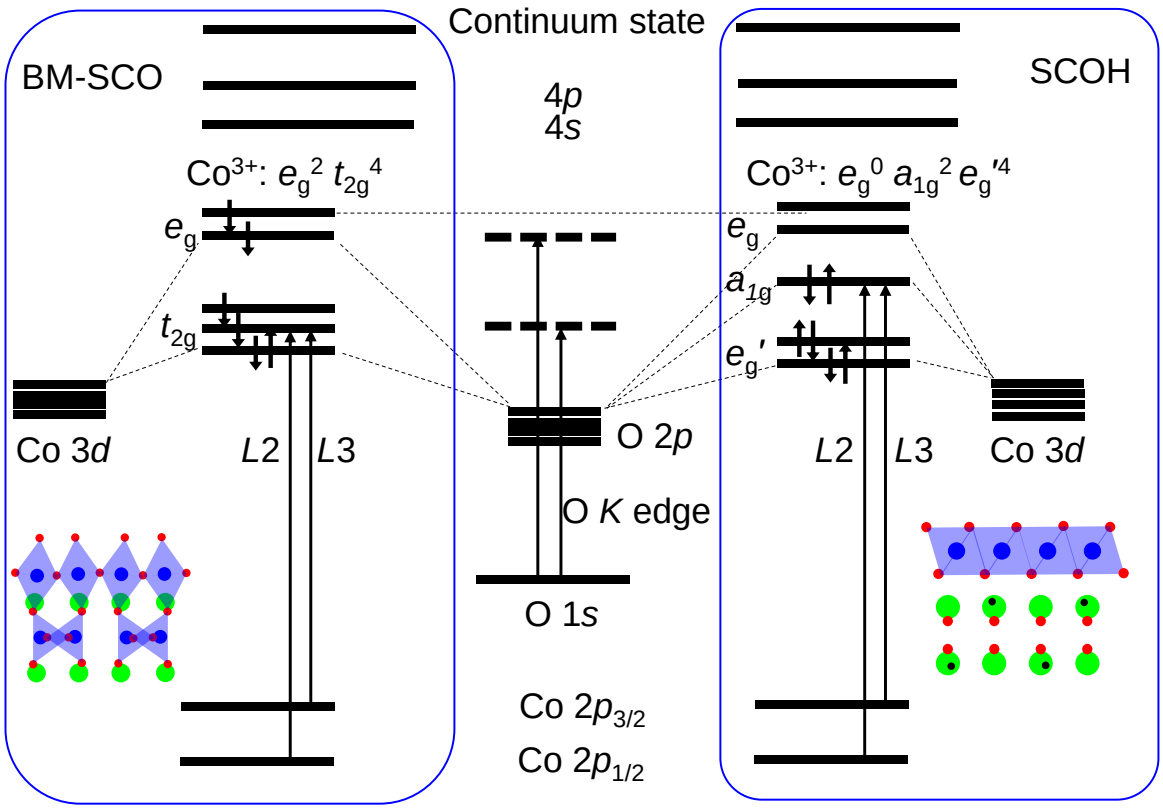

Figure S12. Electronic configuration of Co^{III} -O hybridization in BM-SCO octahedra crystal ligand field (left) and SCOH triangular crystal ligand field (right)

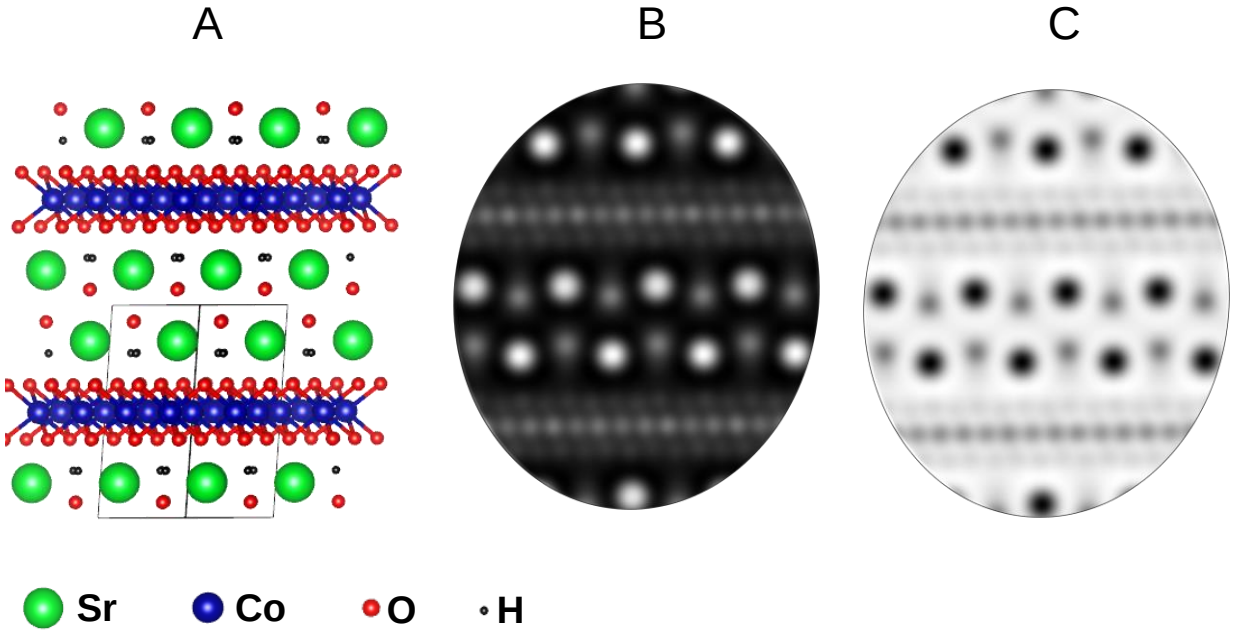

Figure S13. (A) The atomic structure of $SrCoO_3H$ (200) plane. The corresponding simulated HADDF-STEM and ABF image are shown in (B) and (C), respectively. The contrast of H is fairly weak in the ABF image, and its direction observation is thereby a big challenge.

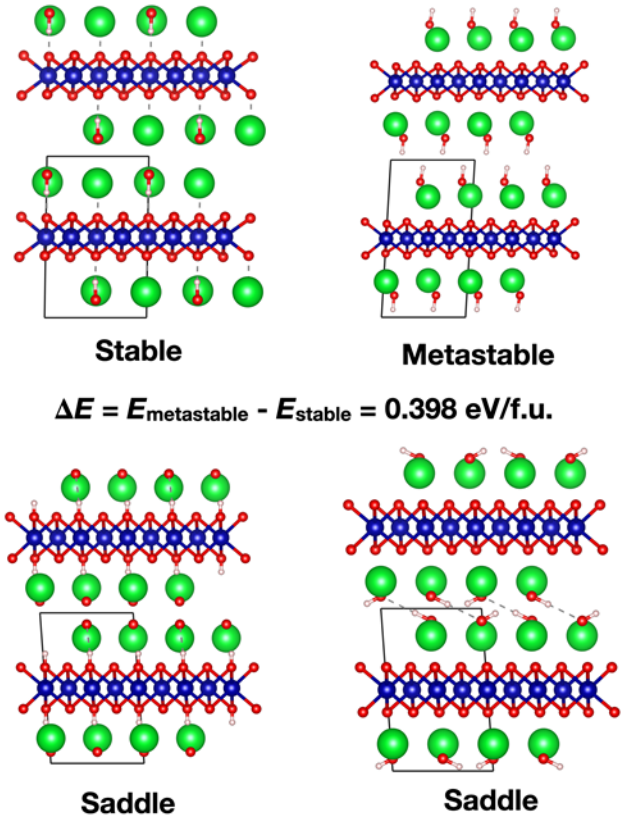

Figure S14. Sketch of the stable and metastable phases determined in the DFT calculations, which are both elastically and vibrationally stable. The energy of the stable phase is about 0.4 eV/f.u. lower than that of the metastable phase. Hydrogen bonds are absent in the metastable phase. Several unstable saddle geometries were found in the simulations for which upon geometry relaxation the H atoms spontaneously moved to the hydrogen positions corresponding to the stable or metastable phases. Sr, Co, O and H atoms are represented with green, blue, red, and pink spheres, respectively.

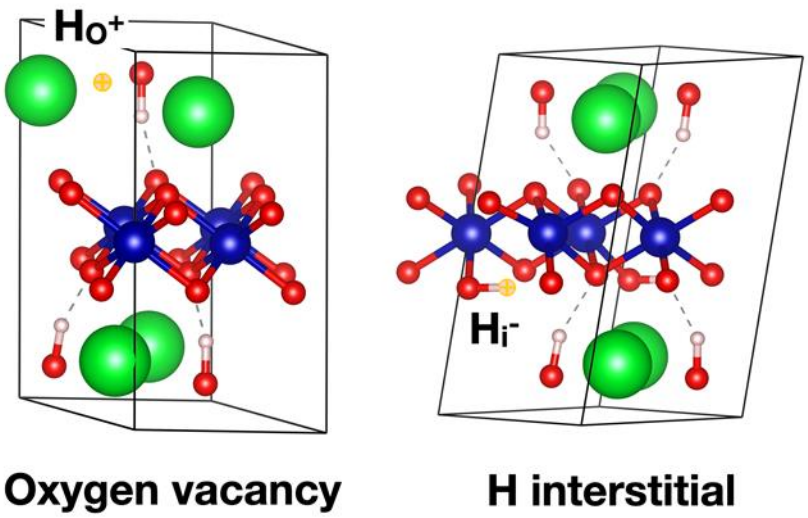

Figure S15. Sketch of the energetically most favorable hydrogen interstitial positions in the presence and absence of oxygen vacancies determined with first-principles simulation methods. In the presence of oxygen vacancies created in SrO layers, the optimal H position corresponds to that of the absent O atom; the corresponding charge state is H_O^+ (i.e., the isolated hydrogen atoms present a deficiency of electronic charge as compared to that of the H atoms in stoichiometric SCOH). The energetically most favorable H position in the absence of oxygen vacancies is located on the CoO_2 layers; the corresponding charge state is H_i^- (i.e., the interstitial hydrogen atom presents an excess of electronic charge as compared to that of the H atoms in stoichiometric SCOH). Sr, Co, O and H atoms are represented with green, blue, red, and pink spheres, respectively. The H interstitial atoms are highlighted in yellow color.

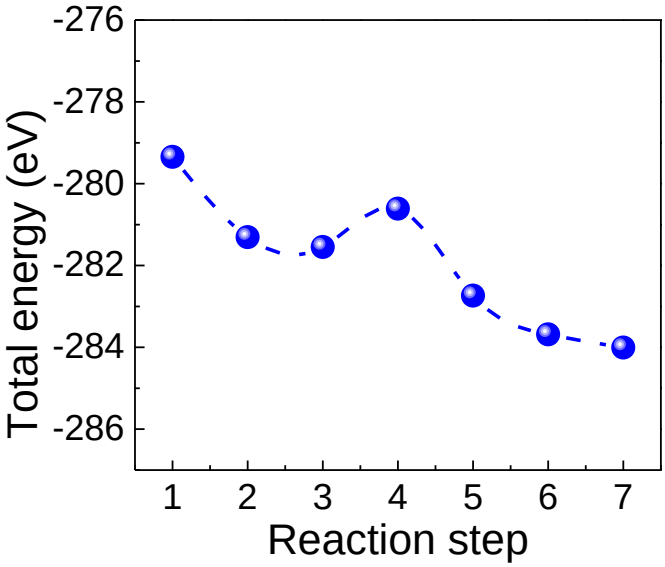

Figure S16. Total energy of the BM-SCO/SCOH supercell during the 7-steps phase transformation illustrated in Figure 3. In order to reveal the role of water in the BM-to-layered phase transition mechanism, we also calculated the total-energy of hydrated BM-SCO/SCOH supercell by first-principle calculations. The initial unit cell of SCOH is composed by 2×2-unit cells of CoO_2, 1×1-unit cells of Sr_2O_2 and 4 H atoms along the x and y directions. The dehydrated structure model consists of 1×1 unit cell of BM-SCO and 2 H_2O molecules. The in-plane lattice parameter (*a* and *b*) of the BM-SCO unit cell are 5.574 Å and 5.470 Å based on experiments, respectively (**Table S1**). The hydrated BM-SCO/SCOH supercell model is constructed by combining a BM-SCO and a SCOH unit cell along the x and y directions. The *a* and *b* of SCOH are 5.01 Å and 5.56 Å based on experiments, respectively. The *a* and *b* of the BM-SCO/SCOH supercell was determined to be 5.428 Å and 5.538 Å according to minimum energy optimization. The vdW-corrected functionals proposed by Grimme DFT+D2 methods were used in first-principles calculations [1]. In the out-of-plane direction, the thickness of the vacuum region is >15 Å to avoid the interactions between neighboring slabs.

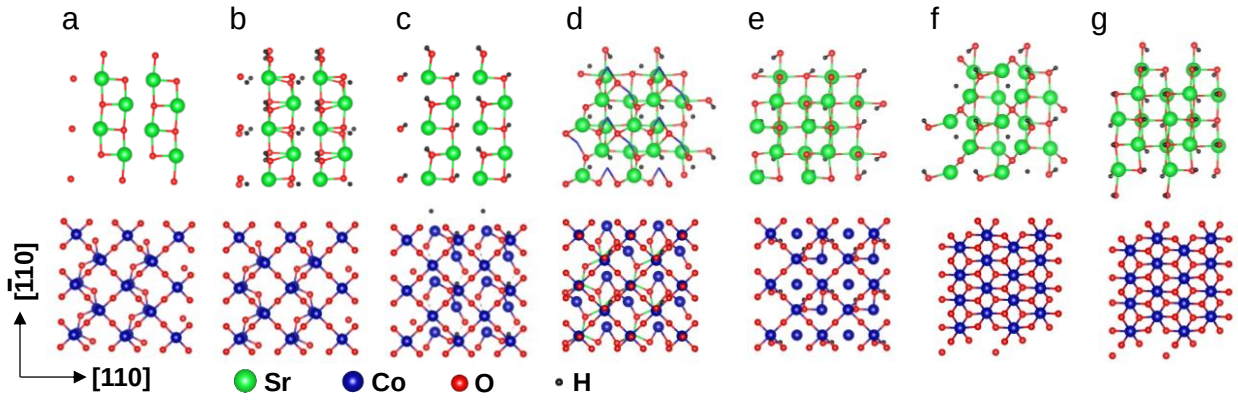

Figure S17. In-plane symmetry change atoms rearrangement of both SrO and CoO layers during the hydration of BM-SCO. These 7 quasi-stable states correspond to Figure 3a)-g) in the manuscript one by one. We selected the 2nd to the 5th M-O (M=Co and Sr) layers from the top in Figure 3 to show how the symmetry changes in in-plane. In Figure S17a)-b), the skeleton of both SrO and CoO layers did not change much before protons intercalate into the CoO layers. Starting from Figure S17c), the Co atoms in the top CoO layer moved to the upper-corner of the bottom Co-Co box, which allowed the top layer Sr atoms shift along the [111] direction in Figure S17d). Then the Co atoms in top layer shifted to the centre of the bottom Co-Co box (Figure S17e)). Till now, the SrO and CoO layers exchanged their positions. The alternative stacking of SrO and CoO layers in BM-SCO changed to two SrO layers and two CoO layers stacking on each other. The neighbouring two CoO layers transformed to a hexagonal CoO_2 layer in Figure S17f), and then the two protonated SrO layers changed to a rock salt $Sr_2O_2H_2$ layer in Figure S17g).

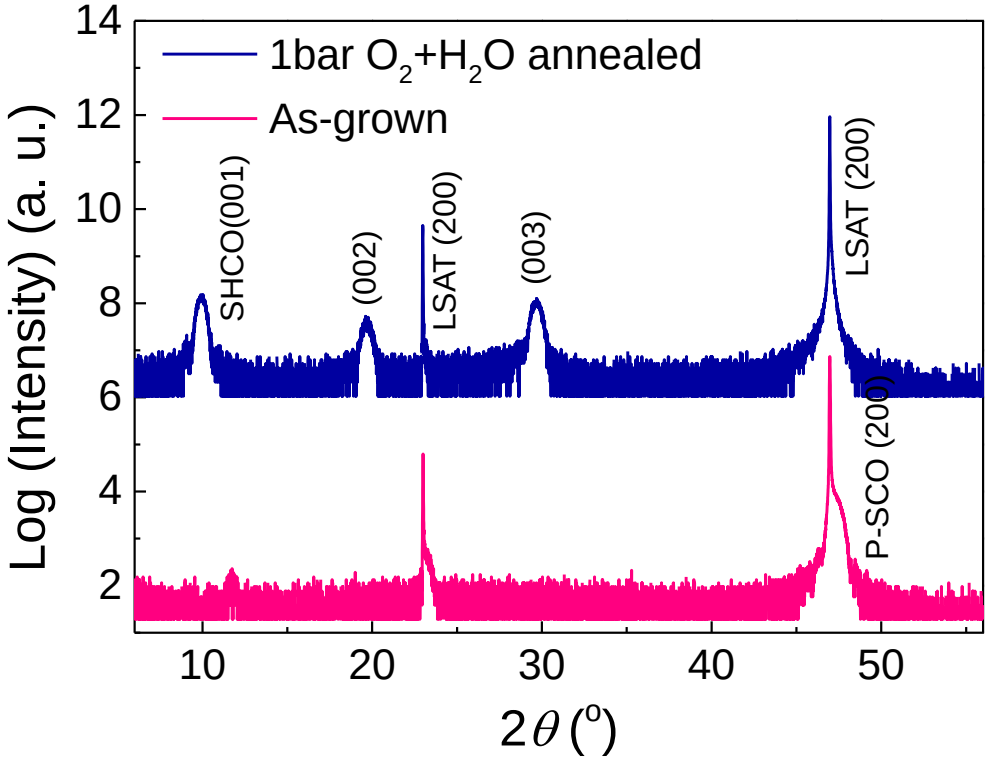

Figure S18. Water vapor annealing on P-SCO thin film grown on (001) LSAT substrate. In 1 bar O_2 + H_2O the perovskite SCO reduced to BM-SCO first and then transformed to SCOH.

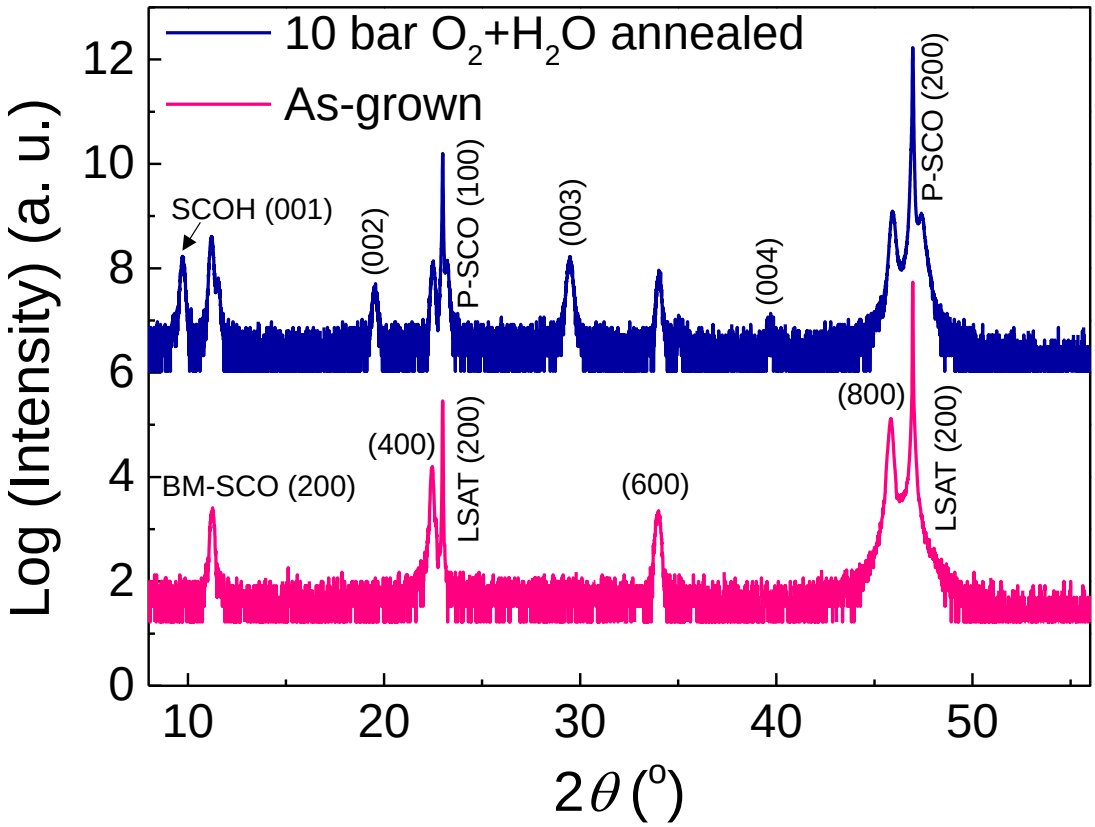

Figure S19. High pressure water vapor annealing on BM-SCO thin film grown on LSAT substrate. The film was 67 nm thick. In 10 bar O_2 + H_2O part of the BM-SCO was oxidized to perovskite which resisted to change to SCOH due the lack of oxygen vacancies.

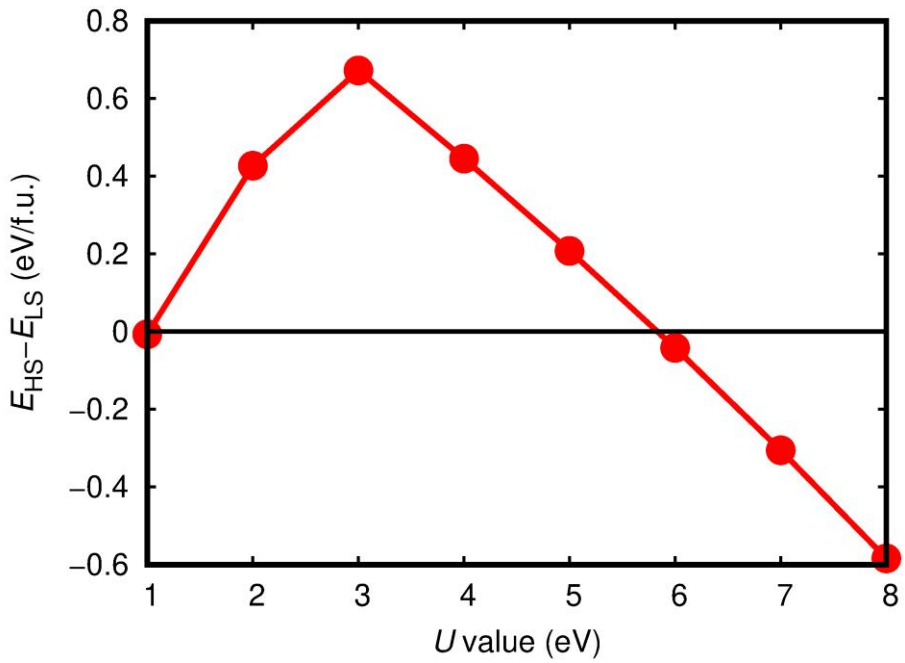

Figure S20. The impact of the selected U parameter value on the energy difference between the Co high-spin (HS) and Co low-spin (LS) states for bulk SCOH. It is found that for $U \geq 6$ eV the Co HS state becomes energetically more favorable than the Co LS state. In view of these theoretical outcomes and our experimental measurements, it is recommended to employ values U < 6 eV for the correct DFT+U theoretical description of bulk SCOH

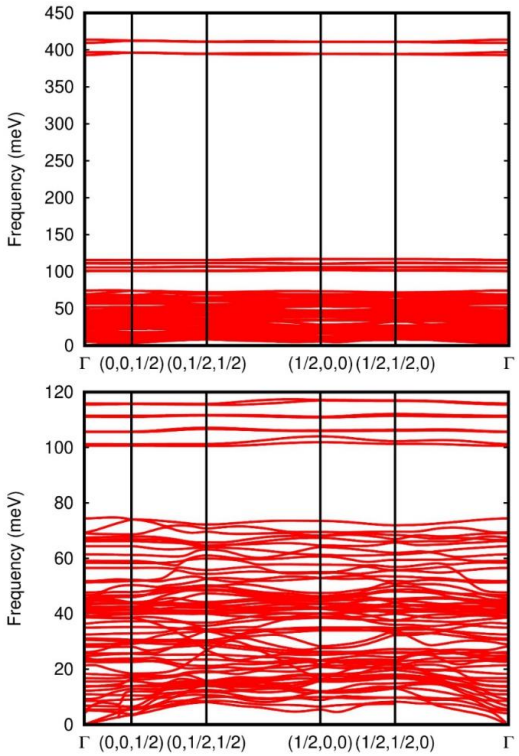

Figure S21. Vibrational phonon spectrum of bulk SCOH calculated with first-principles methods based on density functional theory. The predicted ground-state phase is shown to be vibrationally stable. Bottom panel represents the low and middle-frequency range of the full phonon spectrum. By using DFT methods, we explored several other possible H ions arrangements in which no hydrogen bonds were established with neighbouring O atoms; however, in all those cases it was found that the resulting geometries were either unstable (*i.e.*, spontaneously relaxed to the reported ground state) or metastable (*i.e.*, presented a higher energy than that of the reported ground state). Specifically, the elastic stability criteria for triclinic structures were all fulfilled and the vibrational phonon frequencies were all found to be real.

Table S1. Lattice parameters of SCOH.

	2θ	d [Å]	a [Å]	b [Å]	c [Å]	α [^{o}]	β [^{o}]	γ [^{o}]
BM-SCO			5.574	5.470	15.745	90.0	90.0	90.0
BM pseudo-tetragonal			3.905	3.905	3.936	90.0	90.0	90.0
Sr_2O_2 layer	48.8^o (400)	1.87	7.48	7.48				84.0
Orthogonalized Sr_2O_2 [a)]			5.01	5.56				90.0
CoO_2 layer	35.7^o $(10\bar{1}0)$ 36.8^o $(01\bar{1}0)$	2.51 2.44	2.90	2.82	`			120.0
Orthogonalized CoO_2 [b)]			2.51	2.82				90.0
Triclinic-SCOH			7.48	7.48	9.08	86.3	86.3	84.0
Orthogonalized SCOH			5.01	5.56	9.08	90.0	95.5	90.0

[a)] The a and b of orthogonalized Sr_2O_2 layer is calculated by 7.48×sin (84°/2) and 7.48×cos (84°/2), respectively.

[b)] The a of orthogonalized CoO_2 layer is calculated by 2.90×sin60^o.

References

[1] S. Grimme, *J. Comput. Chem.* **2006**, 27, 1787.